Progress In Electromagnetics Research B, Vol. 56, 347–363, 2013

DESIGN AND ANALYSIS OF TAPERED SLOT ANTENNA WITH 3.5/5.5 GHz BAND-NOTCHED CHARACTERISTICS

Daeheon Lee[1, *], Haeyong Yang[1], and Youngki Cho[2]

[1]The Attached Institute of Electronics and Telecommunications Research Institute, Daejeon, Rep. of Korea

[2]The Department of Electrical Engineering and Computer Science, Kyungpook National University, Daegu, Rep. of Korea

Abstract—A novel tapered slot antenna (TSA) with 3.5/5.5 GHz dual band-notched characteristics for ultra-wideband (UWB) radios is proposed in this paper. To realize dual band-notched characteristics at the TSA, we employ (a) a pair of nested C-shaped stubs beside the feed line and (b) a broadband microstrip-to-slot-line transition with an Archimedean spiral-shaped slot. The proposed antenna has been successfully simulated, implemented, and measured. An equivalent circuit model of the proposed antenna is also presented to discuss the mechanism of the dual band-notched TSA. The measured data for the optimized case show the bandwidth for the VSWR < 2 to be 9.2 GHz (from 2.4 to 11.6 GHz) with two notched bands of 3.1–4.0 GHz (WiMAX band) and 5.1–6.2 GHz (WLAN band), respectively. The measured electrical parameters of the proposed antenna and its radiation patterns show excellent performance with good pulse handling capabilities. Also, the 3.5/5.5 GHz dual band-notched characteristics are achieved without increasing the size of the single band-notched TSA reported previously.

1. INTRODUCTION

Ultra-wideband (UWB) technology has received great attention in the field of wireless communication due to its merits, such as a high data rate, small emission power, and low cost for short range access and remote sensing applications. In UWB radio systems, the UWB antenna is a key component. Researchers have investigated various types of

Received 27 September 2013, Accepted 12 November 2013, Scheduled 12 November 2013

* Corresponding author: Daeheon Lee (leedh@ensec.re.kr).

UWB antennas. Among them, the tapered slot antenna (TSA) [1–6] is a promising candidate as it offers a wide operational bandwidth and planar size that has the advantage of being integrated easily with RF circuits.

The frequency range for UWB systems between 3.1–10.6 GHz causes interference to existing wireless communication systems, such as the world interoperability for microwave access (WiMAX) for IEEE 802.16 operating in the 3.3–3.7 GHz band and wireless local area networks (WLANs) for IEEE 802.11a operating in the 5.15–5.825 GHz band. To mitigate any interference between these coexisting systems, a UWB antenna is needed that has intrinsic filtering properties at their frequencies. To minimize (a) the footprint of the antenna system, (b) the computational complexity of the signal processing, and (c) the cost, it is highly desirable for those filters to be handled intrinsically rather than through any additional external band-stop filter devices. Many designs have been presented in the literature concerning the UWB antenna with band-notched characteristics. Those designs use various types of addition (i.e., slots, slits, and parasitic elements) in the radiator, the ground plane, or even in the feeder to achieve the required band-notched characteristics with limited impact on the required passband [7–16].

Recently, several band-notched TSAs have been studied and discussed [17–20]. In general, the band-notched function can be achieved by attaching a parasitic strip [17, 18] and embedding a couple of slits/slots on the radiator or the microstrip feed line of the antenna [19, 20]. However, all the TSAs mentioned above have only one notched band. Although an elliptical TSA having dual band-notched characteristics for the lower and upper WLAN bands was presented in [21], there still is the potential interference between UWB and WiMAX systems. In this work, a novel TSA with 3.5/5.5 GHz dual band-notched characteristics is proposed for UWB radios. By attaching a pair of nested C-shaped stubs beside the feed line, a single band-notched TSA is first designed. To achieve dual band-notched characteristics in the TSA, a broadband microstrip-to-slot-line transition with an Archimedean spiral-shaped slot is used together with the pair of nested C-shaped stubs. By adjusting the dimensions of the C-shaped stubs properly, a frequency notch at 3.5 GHz can be obtained. Also, by choosing the length of the Archimedean spiral-shaped slot to be about half-wavelength of the notch at 5.5 GHz, the other notched band can be achieved. Another key point of the proposed TSA is that we can tune one notch frequency with little effect on the other because the coupling between the two resonance structures is weak.

The proposed antenna avoids spatial-dependent band-stop

characteristics by introducing a resonance stub and slot on the non-radiating part of the antenna. Besides spatial-independent band-stop characteristics, the 3.5/5.5 GHz dual band-notched characteristics are achieved without increasing the size of the single band-notched TSAs reported previously [22].

In this paper, numerical and experimental results on the frequency notched characteristic, radiation pattern, time-domain performance, gain, and current (field) distribution of the proposed antenna are presented and discussed. Finally, an equivalent circuit model of the proposed dual band-notched TSA is extracted to explain the dual band-notched characteristics.

2. DUAL BAND-NOTCHED TSA DESIGN AND RESULTS

2.1. Antenna Configurations

Figure 1 shows the configuration of the dual band-notched TSA. The proposed slot antenna is fabricated on a low cost FR4 substrate with thickness $h = 0.8$ mm and relative permittivity $\varepsilon_r = 4.4$. The dimensions of the antenna are about 50 mm × 50 mm × 0.8 mm. The width of the microstrip feed line L_m is fixed at 1.46 mm to achieve 50-Ω characteristic impedance. The basic antenna structure consists of a feed line, a microstrip-to-slot-line transition, and a radiating slot. As shown in Figure 1, the microstrip-to-slot-line transition

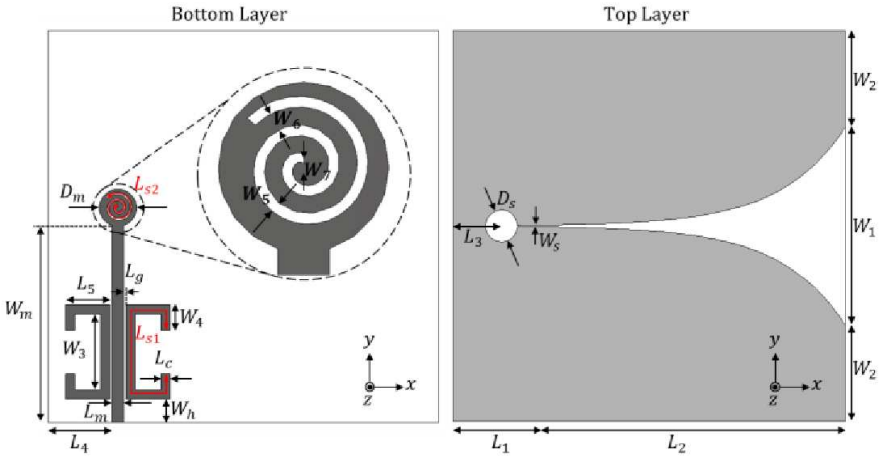

Figure 1. Geometry of the proposed TSA.

is connected to the feed line and the radiating slot, respectively. The microstrip-to-slot-line transition offers a frequency-independent transition characteristic of electromagnetic fields from the microstrip line to the slot-line and vice versa [23]. The exponent slot flare of the radiating slot is determined by using the design method of [1].

Next, to cutoff the 3.3–3.7 GHz band limited by the WiMAX system, a pair of nested C-shaped stubs is placed beside the feed line. By placing the stubs close to the feed line, this resonator is strongly coupled to it. It captures and stores all of the input energy at its resonance frequency; thus, it creates a single band-notched frequency filter. In addition to WiMAX systems, WLAN systems (5.15–5.825 GHz) may also cause interference with UWB systems. To achieve dual band-notched characteristics, a broadband microstrip-to-slot-line transition, having an Archimedean spiral-shaped slot and a pair of nested C-shaped stubs beside the feed line, is adopted to generate notched bands with central frequencies of 5.5 and 3.5 GHz, respectively. Note that, with this design, there is no need to change the dimensions of the original TSA. Rather, each resonance of the stub and slot simply needs to be tuned by adjusting their dimensions to achieve the desired band-notched function. Moreover, these electrically small resonators have a minimal impact on other frequencies [24].

The notched frequency, given the dimensions of the band-notched feature, can be postulated as

$$f_{\text{notch}} = \frac{c}{2L_{s1,2}\sqrt{\varepsilon_{eff}}}, \tag{1}$$

where $L_{s1,2}$ is the total length of the nested C-shaped stubs and the Archimedean spiral-shaped slot, respectively, ε_{eff} the effective dielectric constant, and c the speed of the light. We can take (1) into account in obtaining the total length of the stub and slot at the

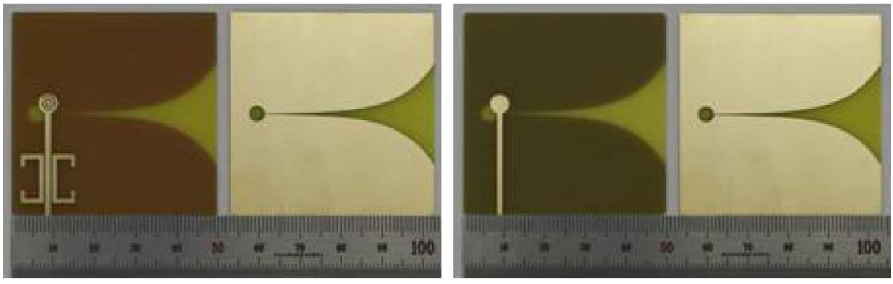

(a) (b)

Figure 2. Photograph of fabricated TSAs: (a) proposed TSA and (b) reference TSA.

very beginning of the design and then adjust the geometry for the final design. The prototype photo of the dual band-notched TSA is shown in Figure 2. Furthermore, an un-notched reference antenna without the stub and slot is also designed, fabricated, and measured for comparison. The optimal antenna geometric parameters are summarized in Table 1.

Table 1. Optimal parameters of the proposed TSA.

Parameter	Value [mm]	Parameter	Value [mm]
W_1	25.2	D_m	4.8
W_2	12.4	D_s	4
L_1	8.5	W_s	0.16
L_2	41.5	W_3	9.6
W_m	25.11	W_4	3.2
L_m	1.46	L_3	6.2
L_4	8.22	L_5	5.7
L_g	0.3	L_c	1.2
W_h	3	W_5	0.3
W_6	0.5	W_7	0.25
L_{s1}	25.7	L_{s2}	14.9

2.2. Results and Discussions

The VSWR performance of the fabricated prototype was measured with an Agilent N5242A vector network analyzer. The simulated and measured VSWR values versus frequency for the dual band-notched TSA and a reference antenna are compared in Figure 3. The designed antenna has an impedance bandwidth of 2.4–11.6 GHz for a VSWR less than 2, except the frequency notched bands of 3.1–4.0 and 5.1–6.2 GHz. Obviously, this measured frequency range covers the commercial UWB band (3.1–10.6 GHz) and rejects the bands of 3.3–3.7 and 5.15–5.825 GHz to overcome electromagnetic interference (EMI) problems between UWB and WiMAX/WLAN systems. There is a discrepancy between the measured data and the simulated results, which were obtained using a time-domain finite integration technique (CST Microwave Studio). This may be caused by a fabrication error and the SMA connector. It is also evident that at higher frequencies there is more sensitivity to fluctuation of the substrate's relative permittivity. As shown in Figure 3, there is another notch at the second-order resonance frequency of the spiral slot around 11.8 GHz [25, 26].

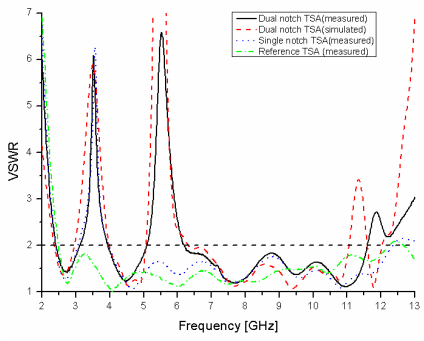

Figure 3. VSWRs of the proposed TSA.

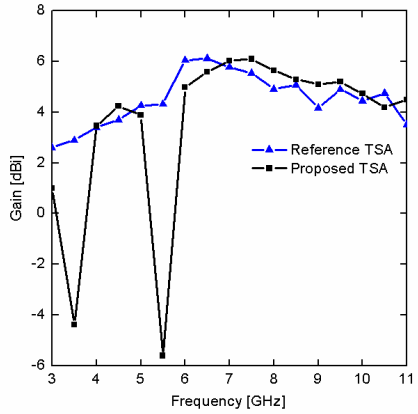

Figure 4. Measured gain of the proposed TSA.

Figure 4 plots the measured gain in the end-fire direction ($+x$) against frequency for the band-notched antenna, compared with that of the reference antenna alone (i.e., without the stub and slot). As desired, two sharp gains decrease in the vicinity of 3.5 and 5.5 GHz. However, for other frequencies outside the rejected bands, the antenna gain is similar to the corresponding value of the reference antenna. This confirms that the proposed antenna provides a high level of rejection to signals within the notched bands without sacrificing pass band performance.

The normalized simulated and measured far-field radiation patterns of the proposed antenna in the E-plane (xy-plane) and H-plane (xz-plane) for Co- and X-polarization at frequencies of 3.1, 7.0, and 9.0 GHz are plotted in Figure 5, respectively. As shown in the figure, a reasonable agreement between the measured and simulated Co-polarization is observed across the whole frequency band, and the antenna features end-fire properties. The radiation patterns remain relatively stable over the operating frequency range. Furthermore, the cross-polarization level is less than -20 dB in the end-fire direction across the whole frequency band.

Figure 6 shows the simulated current distributions of our proposed antenna at frequencies of 3.1, 3.5, 5.5, and 9.0 GHz for the optimal design. The large current distribution is indicated in red and the small one is indicated in green. The current distribution is relatively constant at 3.1 and 9.0 GHz. It may be concluded that the patterns at these two frequencies will be very similar to each other, as conventional

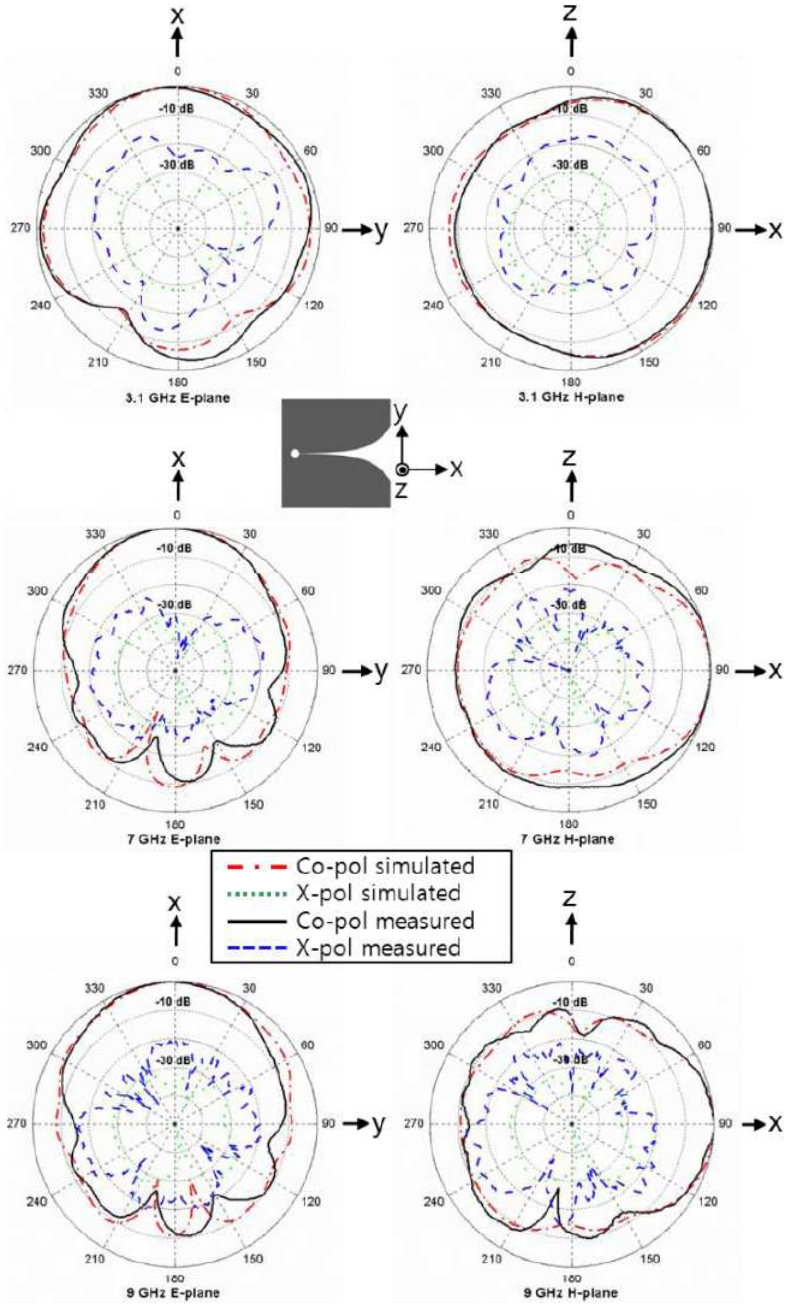

Figure 5. Simulated and measured radiation patterns at various frequencies.

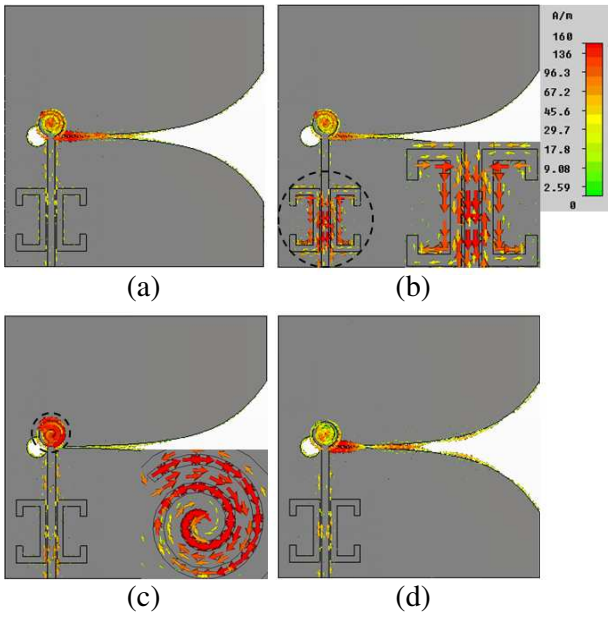

Figure 6. Simulated current distributions of the proposed TSA: (a) $f = 3.1\,\text{GHz}$, (b) $f = 3.5\,\text{GHz}$, and (c) $f = 5.5\,\text{GHz}$, $f = 9.0\,\text{GHz}$.

TSAs behave. However, as shown in Figures 6(b) and (c), the current distributions around the pair of nested C-shaped stubs and the Archimedean spiral-shaped slot increase significantly at 3.5 and 5.5 GHz, which implies that the stubs and slot resonate near 3.5 and 5.5 GHz, respectively. In these structures at the notch frequency, the current flows are oppositely directed between the interior and exterior edges. Therefore, the resultant radiation fields cancel out, and high attenuation near the notch frequency is produced.

The other important parameter for the UWB antennas, especially when used to send/receive pulsed signals, is the time domain response. For this purpose, two antennas are put at a distance of one meter such that their tapered slots face each other. For comparison, the proposed dual band-notched antenna and the reference antenna are connected as the receive antenna, respectively. The time domain characteristics of the fabricated prototype were measured with a Tektronix DSA 71254B oscilloscope. Figure 7 shows the received pulse with small distortions and ringing effects, which is similar to the second-order differentiated transmit pulse. The measured results demonstrate that this type of antenna is well suited for the impulse response.

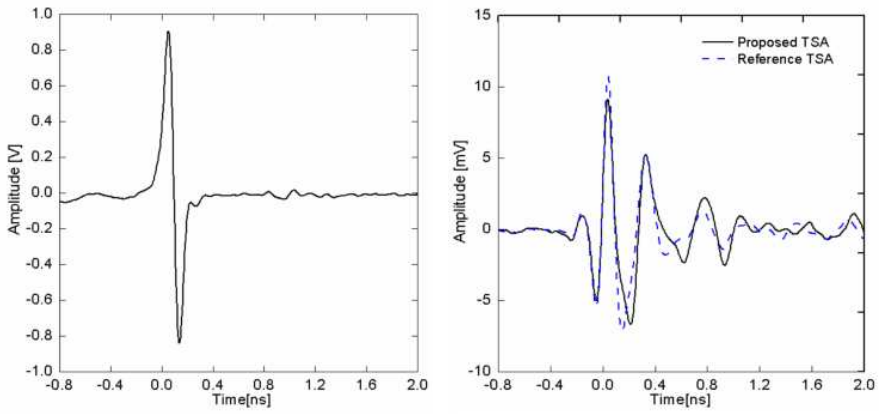

(a) (b)

Figure 7. Time-domain characteristic of the proposed TSA: (a) measured transmit pulse and (b) measured received pulse.

2.3. Parametric Studies of Proposed Antenna

Every geometric parameter has different effects on the performance of the proposed antenna. In this subsection, in relation to the desired band-notched function, the effects of the spiral-shaped slot and C-shaped stub parameter on the antenna's performance are discussed. As shown in Figure 1, L_{s1} and L_{s2} mean the length of the nested C-shaped stubs and the Archimedean spiral-shaped slot, respectively. Figure 8 shows the simulated VSWRs of the proposed antenna for the C-shaped stub lengths $L_{s1} = 25.7$, 26.2, and 26.7 mm with the final design values of other dimensions. The center frequency of the 3.5 GHz notched band

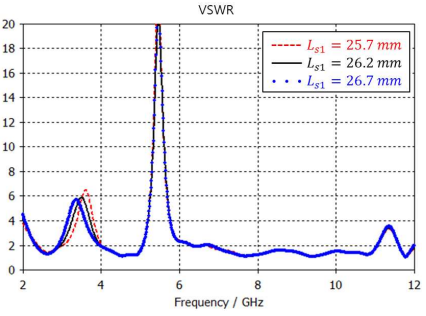

Figure 8. Effect of parameter L_{s1} of the C-shaped stubs on the band-notched characteristics.

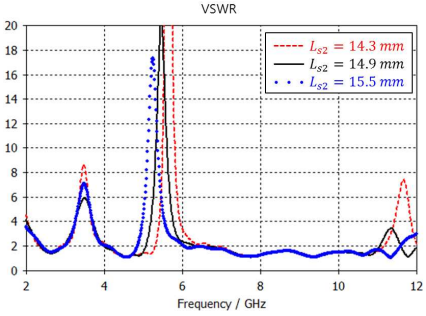

Figure 9. Effect of parameter L_{s2} of the spiral-shaped slot on the band-notched characteristics.

is shifted toward lower frequencies by increasing the stub length L_{s1}. Figure 9 shows the simulated VSWRs of the proposed antenna for the spiral-shaped slot lengths $L_{s2} = 15.5$, 14.9, and 14.3 mm. As the length L_{s2} of the slot decreases from 15.5 to 14.3 mm, the center frequency of the 5.5 GHz notched band varies from 5.2 to 5.6 GHz. Based on the above analysis, it is clear that these two notch bands can be tuned and controlled independently.

3. EQUIVALENT CIRCUIT MODEL OF PROPOSED ANTENNA

In this section, to discuss the mechanism of the dual band-rejected filtering properties, an equivalent circuit model of the proposed dual band-notched UWB antenna is presented. Conceptually, the microstrip and slot-line are viewed as a transmission line with characteristic impedance Z_0. For simplicity, the radiating element of the UWB antenna can be represented by a radiation resistance. The microstrip-to-slot-line transition can be modeled by the 4th-order Marchand balun circuit [27]. The nested C-shaped stubs and Archimedean spiral-shaped slot are modeled as a series and shunt stub, respectively.

3.1. Transmission Line Models for Microstrip and Slot-line

In the equivalent circuit model, the microstrip and slot-line can be simply represented by a transmission line with characteristic impedance Z_0. Closed-form expressions for the effective dielectric constant and characteristic impedance of the microstrip and slot-line are given in [27, 28], respectively.

3.2. Equivalent Circuit Model for Proposed Antenna

The equivalent circuit model for the proposed dual band-notched antenna of Figure 1 is shown in Figure 10. The 4th-order Marchand balun circuit as a two-port circuit consists of (a) two microstrip lines with Z_1, Z_2, and an open-ended microstrip reactance X_m, (b) two slot-lines with Z_3, Z_4, and a shorted slot-line impedance R_s and X_s, (c) turns-ratio of transformer n, (d) series and shunt stubs for the C-shaped stubs and spiral-shaped slot, and (e) a radiation resistance Z_{ant} as a load.

Using the $ABCD$ transmission parameters, the overall T_B matrix of the balun as a two-port circuit can be obtained by the following expression:

$$T_B = T_1 \cdot T_2 \cdot T_n \cdot T_3 \cdot T_4, \tag{2}$$

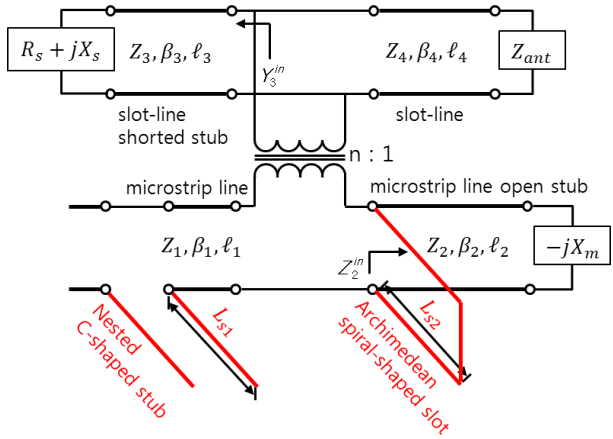

Figure 10. Equivalent circuit model for the proposed antenna.

where $T_{1,4} = \begin{bmatrix} \cos\beta_{1,4}\ell_{1,4} & j\sin\beta_{1,4}\ell_{1,4} \\ jY_{1,4}\sin\beta_{1,4}\ell_{1,4} & \cos\beta_{1,4}\ell_{1,4} \end{bmatrix}$, $T_n = \begin{bmatrix} n & 0 \\ 0 & 1/n \end{bmatrix}$, $T_2 = \begin{bmatrix} 1 & Z_2^{in} \\ 0 & 1 \end{bmatrix}$, $T_3 = \begin{bmatrix} 1 & 0 \\ Y_3^{in} & 1 \end{bmatrix}$.

The impedance Z_2^{in} and admittance Y_3^{in} for the open end and shorted stubs are expressed as follows:

$$Z_2^{in} = Z_2 \frac{-jX_m + jZ_2 \tan\beta_2\ell_2}{Z_2 + X_m \tan\beta_2\ell_2}, \tag{3}$$

$$Y_3^{in} = Y_3 \frac{Z_3 + j(R_s + jX_s)\tan\beta_3\ell_3}{(R_s + jX_s) + jZ_3 \tan\beta_3\ell_3}. \tag{4}$$

where β_i and ℓ_i are the propagation constant and length of each element at the operating frequency.

Das [29] has derived a simple closed-form expression for turns ratio n after making a number of approximations in the analysis. This expression is given as

$$n = \frac{J_0(\beta_4\ W_1/2)\, J_0(\beta_1\ W_4/2)}{\beta_4^2 + \beta_1^2} \times \left[\frac{\beta_1^2 k_2 \varepsilon_r}{k_2\varepsilon_r \cos k_1 h - k_1 \cos k_1 h} + \frac{\beta_4^2 k_1}{k_1 \cos k_1 h - k_1 \sin k_1 h} \right], \tag{5}$$

where $J_o(\cdot)$ is the zeroth-order Bessel function and

$$k_1 = k_0\sqrt{|\varepsilon_r - \varepsilon_{eff4} - \varepsilon_{eff1}|}, \quad k_2 = k_0\sqrt{|\varepsilon_{eff4} + \varepsilon_{eff1} - 1|}. \tag{6}$$

Here, ε_{eff1} and ε_{eff4} are the effective dielectric constants, and W_1 and W_4 are the widths of the microstrip line and slot-line, respectively. The overall scattering matrix for the balun which has different two-port impedance is then readily obtained.

3.3. Equivalent Circuit Model for C-Shaped Stubs

The C-shaped stubs can be represented by the capacitance network shown in Figure 11. Here, C_m represents the capacitance of the two microstrip conductors in the absence of the ground conductor, while C_{s1} and C_{s2} represent the capacitance between the microstrip conductor and ground, in the absence of the other microstrip conductor. For microstrip lines, the capacitances per unit length of line can be obtained numerically or by approximate quasi-static techniques [27]. The input impedance of the parallel RLC resonator is calculated as follows:

$$\begin{aligned} R &= \frac{Z_0}{\alpha L_{s1}} = \frac{Z_0}{(\alpha_c + \alpha_d) L_{s1}} \cong 30\,\mathrm{k\Omega}, \\ C_{eq} &\cong 6.20\,\mathrm{pF}, \\ L_{eq} &\cong \frac{1}{\omega_0^2 C_{eq}} \cong 0.34\,\mathrm{nH}, \end{aligned} \tag{7}$$

where R, C_{eq}, and L_{eq} indicate the resistance, capacitor, and inductor values of the C-shaped stubs, respectively. Here, α_c and α_d are the attenuation factors due to conductor and dielectric loss, respectively.

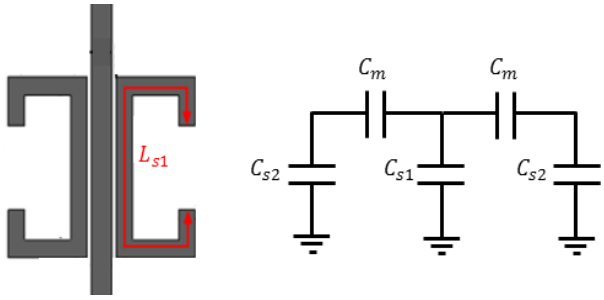

Figure 11. C-shaped stubs and their equivalent capacitance network.

3.4. Equivalent Circuit Model for Spiral-shaped Slot

The equivalent circuit for the Archimedean spiral-shaped slot is shown in Figure 12 [30]. In summary, filtering characteristics of the spiral-shaped slot can be analyzed using the LC equivalent circuit model.

When a time varying electric field penetrates the spiral-shaped slot specifically, a current can be induced along the spiral-shaped slot. Then, a distributed inductance is generated in proportion to the length of the spiral-shaped slot, and a mutual inductance is also generated between the lines of the spiral-shaped slot. Distributed capacitance between inside and outside lines and fringing capacitances between lines and ground conductor are generated. These fringing capacitances are equivalently connected in parallel. Consequently, the equivalent circuit model of the spiral-shaped slot can be represented as Figure 12.

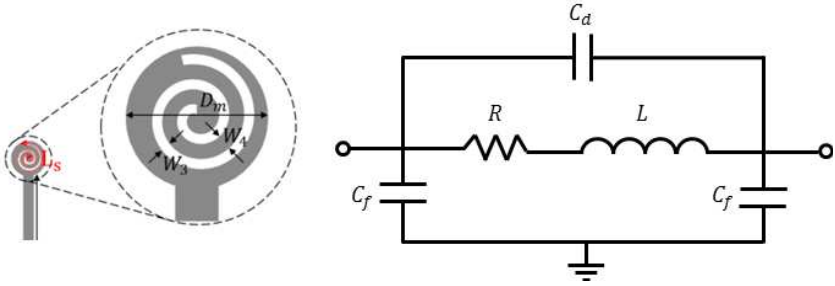

Figure 12. Equivalent circuit model of spiral-shaped slot.

The circuit parameters of C_d, R, L, and C_f are the distributed capacitance, resistance of the spiral line, distributed inductance (mutual inductance is included), and fringing capacitance, respectively. As can be seen in Figure 12, the equivalent circuit of the spiral-shaped slot corresponds to the LC equivalent circuit model of a bandstop filter. The resonance frequency can be estimated as

$$\omega_0 = \frac{1}{\sqrt{LC_T}}, \tag{8}$$

where C_T is the sum of the distributed capacitance and fringing capacitance, and L is sum of the distributed inductance and mutual inductance.

Finally, the comparison between the simulated VSWR of the proposed TSA by CST and by the equivalent circuit model of Figure 10 is shown in Figure 13. As seen in the figure, the trends of the curves agree reasonably well over the UWB band, especially in the dual notched frequency bands. Although distributed models are often believed to be more accurate than lumped-element models, in this case both models provide very good accuracy. In conclusion, this model is suitable for the proposed dual band-notched TSA.

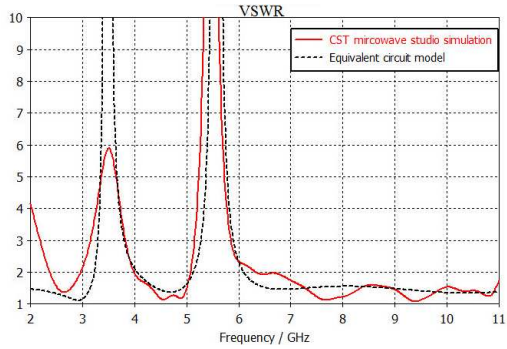

Figure 13. Comparison between the simulated VSWR of the proposed TSA by CST and by the equivalent circuit model.

4. CONCLUSION

A novel dual band-notched UWB TSA was proposed in this paper. The first notched band, which is intended to prevent any interference with existing WiMAX systems, is achieved by using a pair of nested C-shaped stubs beside the feed line. The second notched band, which is intended to prevent interference with 5 GHz WLAN systems, is achieved by a broadband microstrip-to-slot-line transition with an Archimedean spiral-shaped slot. The stubs and slot act independently, and their addition to the antenna does not change the behavior of the original TSA. To discuss the mechanism of the filtering properties, an equivalent circuit model based on the analysis of resonance phenomena has been proposed. The circuit accurately approximates the input impedance of the antenna at all frequencies, and its results are similar to those of full-wave simulation. Parametric studies of the proposed antenna with dual band-notched characteristics can provide guidelines on how to control the band-notched frequencies. The designed antenna is small and has a simple configuration. In addition, the measured results demonstrate that the newly proposed configuration is suitable for the impulse response. From the above results, it may be concluded that the proposed antenna is a good candidate for various UWB applications.

REFERENCES

1. Janaswamy, R. and D. H. Schaubert, "Analysis of the tapered slot antenna," *IEEE Trans. on Antennas and Propag.*, Vol. 35, No. 9, 1058–1065, 1987.

2. Ma, T. G. and S. K. Jeng, "Planar miniature tapered-slot-fed annular slot antennas for ultrawide-band radios," *IEEE Trans. on Antennas and Propag.*, Vol. 53, No. 3, 1194–1202, 2005.
3. Abbosh, A. M., "Miniaturized microstrip-fed tapered-slot antenna with ultrawideband performance," *IEEE Antennas Wireless Propag. Lett.*, Vol. 8, 690–692, 2009.
4. Jolani, F., G. R. Dadashzadeh, M. Naser-Moghadasi, and A. M. Dadgarpour, "Design and optimization of compact balanced antipodal vivaldi antenna," *Progress In Electromagnetics Research C*, Vol. 9, 183–192, 2009.
5. Yao, Y., M. Liu, W. Chen, and Z. Feng, "Analysis and design of wideband widescan planar tapered slot antenna array," *IET Microw. Antennas Propag.*, Vol. 4, No. 10, 1632–1638, 2010.
6. Hamid, M. R., P. S. Hall, P. Gardner, and F. Ghanem, "Switched WLAN-wideband tapered slot antenna," *Electron. Lett.*, Vol. 46, No. 1, 23–24, 2010.
7. Schantz, H. G., G. Wolenec, and E. M. Myszka, III, "Frequency notched UWB antennas," *Proc. IEEE Ultra Wideband Sys. Tech. Conf.*, 214–218, Nov. 2003.
8. Kalteh, A. A., G. R. DadashZadeh, M. Naser-Moghadasi, and B. S. Virdee, "Ultra-wideband circular slot antenna with reconfigurable notch band function," *IET Microw. Antennas Propag.*, Vol. 6, No. 1, 108–112, 2012.
9. Kim, C. B., J. S. Lim, J. S. Jang, Y. H. Jung, H. S. Lee, and M. S. Lee, "Design of the wideband notched compact UWB antenna," *APMC 2007 (2007 Asia-Pacific Microwave Conference)*, 1–4, Dec. 2007.
10. Mehranpour, M., J. Nourinia, C. Ghobadi, and M. Ojaroudi, "Dual band notched square monopole antenna for ultrawideband applications," *IEEE Antennas Wireless Propag. Lett.*, Vol. 11, 172–175, 2012.
11. Lee, J.-H. and Y.-J. Sung, "Band-notched ultra-wideband antenna with asymmetric coupled-line for WLAN and X-band military satellite," *Journal of Electromagnetic Engineering and Science*, Vol. 13, No. 1, 34–37, Mar. 2013.
12. Peng, L. and C. L. Ruan, "UWB band-notched monopole antenna design using electromagnetic-bandgap structures," *IEEE Tran. on Microwave Theory and Tech.*, Vol. 59, No. 4, 1074–1081, 2011.
13. Peng, L. and C.-L. Ruan, "Design and time-domain analysis of compact multi-band-notched uwb antennas with EBG structures," *Progress In Electromagnetics Research B*, Vol. 47, 339–357, 2013.

14. Zhang, Y., W. Hong, C. Yu, Z. Q. Kuai, Y. D. Don, and J. Y. Zhou, "Planar ultrawideband antennas with multiple notched bands based on etched slots on the patch and/or split ring resonators on the feed line," *IEEE Trans. on Antennas and Propag.*, Vol. 56, No. 9, 3063–3068, 2008.
15. Kim, D. O., N. I. Jo, D. M. Choi, and C. Y. Kim, "Design of the novel band notched UWB antenna with the spiral loop resonators," *PIERS Online*, Vol. 6, No. 2, 173–176, 2006.
16. Bao, X. L. and M. J. Ammann, "Printed UWB antenna with coupled slotted element for notch-frequency function," *International Journal of Antennas and Propagation*, 1–7, 2008.
17. Song, Y., Y.-C. Jiao, T.-L. Zhang, G. Zhao, and F.-S. Zhang, "Small tapered slot antenna with a band-notched function for wireless applications," *Progress In Electromagnetics Research Letters*, Vol. 10, 97–105, 2009.
18. Zhu, F., S. Gao, A. T. S. Ho, R. A. Abd-Alhameed, C. H. See, J. Li, and J. Xu, "Miniaturized tapered slot antenna with signal rejection in 5–6-GHz band using a balun," *IEEE Antennas Wireless Propag. Lett.*, Vol. 11, 507–510, 2012.
19. Yoon, I. J., H. Kim, H. K. Yoon, Y. J. Yoon, and Y. H. Kim, "Ultra-wideband tapered slot antenna with band cutoff characteristic," *Electron. Lett.*, Vol. 41, No. 11, 629–630, 2005.
20. Ma, T. G. and S. K. Jeng, "A planar tapered-slot-fed annular slot antenna with band-notched characteristics for ultra-wideband radios," *IEICE Trans. Fundamentals*, Vol. E88-A, No. 9, 2384–2386, 2005.
21. Zhu, F., S. Gao, A. T. S., Ho, R. A. Abd-Alhameed, C. H. See, J. Li, and J. Xu, "Dual band-notched tapered slot antenna using $\lambda/4$ band-stop filters," *IET Microw. Antennas Propag.*, Vol. 6, No. 15, 1665–1673, 2012.
22. Lee, D. H., H. Y. Yang, and Y. K. Cho, "Tapered slot antenna with band-notched function for ultrawideband radios," *IEEE Antennas Wireless Propag. Lett.*, Vol. 5, 495–498, 2012.
23. Schüppert, B., "Microstrip/slotline transition: Modeling and experimental investigation," *IEEE Trans. on Microwave Theory and Tech.*, Vol. 36, No. 8, 1272–1282, 1988.
24. Lin, C. C., P. Jin, and R. W. Ziolkowski, "Single, dual, and tri-band-notched ultrawideband (UWB) antennas using capacitively loaded loop (CLL) resonators," *IEEE Trans. on Antennas and Propag.*, Vol. 60, No. 1, 102–109, 2012.

25. Antonino-Daviu, E., M. Cabedo-Fabrés, M. Ferrando-Bataller, and V. M. Rodrigo-Peñarrocha, "Modal analysis and design of band-notched uwb planar monopole antennas," *IEEE Trans. on Antennas and Propag.*, Vol. 58, No. 5, 1457–1467, 2010.
26. Dissanayake, T. and K. P. Esselle, "Prediction of the notch frequency of slot loaded printed UWB antennas," *IEEE Trans. on Antennas and Propag.*, Vol. 55, No. 11, 3320–3325, 2007.
27. Gupta, K. C., R. Garg, and I. J. Bahl, *Microstrip Lines and Slotlines*, Artech House, Norwood, MA, 1979.
28. Pozar, D. M., *Microwave Engineering*, 2nd Edition, John Wiley & Sons, Inc., 1998.
29. Das, N. K., "Generalized multiport reciprocity analysis of surface-to-surface transitions between multiple printed transmission lines," *IEEE Tran. on Microwave Theory and Tech.*, Vol. 41, No. 6, 1164–1177, 1993.
30. Schmückl, F. J., "The method of lines for the analysis of rectangular spiral inductors," *IEEE Tran. on Microwave Theory and Tech.*, Vol. 54, No. 4, 1183–1186, Apr. 2006.